BIOCELL

Tech Science Press

http://doi.org/10.32604/biocell.2026.077797

ARTICLE

Modulating the Biological Processes and Glycolysis of Hepatocellular Carcinoma Cells by UBR7's Suppression of Pyruvate Kinase PKM2

Bo Liu and Xue Li*

Department of Operating Room, The First Hospital of China Medical University, No. 155, North Nanjing Street, Heping District, Shenyang, China
*Corresponding Author: Xue Li. Email: 18240453032@163.com

Received: 17 December 2025; Accepted: 16 March 2026; Published: 29 June 2026

ABSTRACT: Background: As a key glycolytic enzyme, Pyruvate kinase M2 (PKM2), which is highly expressed in cancer cells, promotes hepatocellular carcinoma (HCC) proliferation/metastasis. This research investigates the involvement of Ubiquitin protein ligase E3 component N-recognin 7 (UBR7) in HCC progression/glycolysis and its potential mechanisms. **Methods:** UBR7 expressions in HHL-5, Huh-7, and HepG2 cells were investigated using Quantitative Reverse Transcription Polymerase Chain Reaction and Western Blot. Cell counting kit-8, clone formation experiment, scratch-wound assay, and transwell testing were conducted to assess the malignant biological behaviors of HepG2 and Huh-7 cells; the absorption level of glucose and generation levels of lactic acid and ATP were tested by assay kits. Huh-7 cells with stably overexpressed or knocked down UBR7 were inoculated into nude mice. Regular measurements were conducted on the tumor size, the tumors were isolated and weighed on the 35th day, and the glycolytic level in the tumor tissues was determined. **Results:** In HCC cells, UBR7 was significantly downregulated. Notably, UBR7 knockdown promoted HCC progression and glycolysis, increasing the viability of HepG2 and Huh-7 cells by 23%–24% ($p < 0.001$), whereas UBR7 overexpression exerted the opposite inhibitory effects, resulting in a reduction of about 19%–31% in cell viability ($p < 0.001$). UBR7 knockdown upregulated PKM2 expression in HCC cells, while UBR7 overexpression led to a marked reduction in PKM2 levels. Importantly, PKM2 overexpression partly abrogated the inhibitory impacts of UBR7 on HCC progression and glycolysis. *In vivo* experiments further demonstrated that UBR7 overexpression suppressed tumor growth and hindered glycolysis in nude mice. **Conclusion:** UBR7 suppressed PKM2 expression, thus hindering malignant biological progression and glycolysis in HCC, providing a potential therapeutic target for HCC treatment.

KEYWORDS: Ubiquitin protein ligase E3 component N-recognin 7; pyruvate kinase M2; hepatocellular carcinoma; glycolysis

1 Introduction

As a major malignant tumor worldwide, primary liver cancer newly affected about 906,000 people in 2020, where 75%–85% of them were in the condition of hepatocellular carcinoma (HCC) [1]. Despite the great contribution of advanced modern medical equipment and technologies to HCC diagnosis and treatment, the prognosis of this condition remains sub-optimal, evidenced by the increasing incidence and mortality [2,3]. It is estimated that HCC cases will increase from 905,700 in 2020 to 1.4 million in 2040 [4]. To better improve the early HCC diagnosis and treatment, it is necessary to further understand the expression changes of cytokines and signaling pathways during the initiation and progression of HCC,

and uncover the interconnections between different genes [5]. Based on this, more effective diagnostic and therapeutic intervention strategies can be devised for this condition.

In the carcinogenic process, cells experience "glutamine addiction", lipid metabolism reprogramming, and dysregulated glycolysis. Hence, regulating cancer cell metabolism becomes a highly promising approach to resisting cancer [6]. The development of a tumor requires sufficient supplies of oxygen and nutrients *in vivo* [7]. As the foremost energy substrate in cells, glucose, even under aerobic conditions, experiences enhanced glycolysis, a process identified as the Warburg effect (i.e., aerobic glycolysis) [8,9]. Abundant lactic acid generated from aerobic glycolysis can be carried to the space outside the cells by monocarboxylate transporters (MCTs); thus, an acidic environment is formed outside the cell, driving the immune evasion, multiplication, attack, and metastasis of tumor cells [10,11]. The last stage of glycolysis is catalyzed by pyruvate kinase (PK), which transfers a high-energy phosphate group from phosphoenolpyruvate to ADP to form pyruvate and ATP. Pyruvate kinase M2 (PKM2), belonging to a subtype of PK, is the main variant promoting cancer cell multiplication [12,13]. PKM2 exhibits heterogeneity, making it adaptable to varying pathological conditions [14,15]. As established, PKM2 is overexpressed in varying cancer cells, including HCC cells, facilitating tumor cell multiplication and metastasis [16–18].

Ubiquitination is the process by which a ubiquitin molecule covalently binds to specific lysine residues of a substrate protein in the presence of a series of ubiquitin-activating enzymes [19]. In recent years, the reprogramming of cancer metabolism regulated by ubiquitination and deubiquitination has garnered increasing attention due to its crucial role in aerobic glycolysis of cancer cells [20–22]. Ubiquitin protein ligase E3 component N-recognin 7 (UBR7) is a member of the UBR family. It harbors a unique plant homeodomain at its C-terminus that is capable of reading histone codes, endowing it with the dual biological functions of mediating ubiquitination modification of non-histone proteins and regulating chromatin epigenetic modification [23,24]. It has been shown that UBR7 expression is down-regulated in pancreatic ductal adenocarcinoma cells and mediates gemcitabine resistance in pancreatic ductal adenocarcinoma cells through ubiquitination of PRMT5, whereas knockdown of UBR7 promotes tumor progression and glycolysis [25]. However, the biological function and regulatory mechanism of the UBR7 in HCC metabolism and malignant progression remain largely unknown. We hypothesize that UBR7 may modulate HCC glycolysis and tumor progression by targeting PKM2. The present study was designed to investigate the expression pattern of UBR7 in HCC, explore its effects on HCC cell proliferation and glycolysis *in vitro* and tumor growth *in vivo*, and clarify the functional relationship between UBR7 and PKM2 in HCC advancement. This study enhances the understanding of UBR7's regulatory mechanisms in the evolution of HCC, driving the development of promising therapeutic drugs and methods for HCC.

2 Materials and Methodology

2.1 Cultivation of the Cells

Human normal liver cell line HHL-5 cells (YS1276C) were obtained from Yaji Biotechnology Co., Ltd. (Shanghai, China); HCC cells Huh-7 (SNL-085), Li-7 (SNL-353), HCC-LM3 (SNL-166), and HepG2 (SNL-083) were bought from Wuhan Sunncell Biotechnology (Wuhan, China). All cell lines were authenticated by short tandem repeat (STR) profiling and confirmed to be negative for mycoplasma contamination. RPMI-1640 medium (SNM-001E, Wuhan Sunncell Biotechnology) was blended with 10% fetal bovine serum (SNS-001, Wuhan Sunncell Biotechnology) and used to culture the cells. Then, the cells were cultivated at a constant temperature (37°C) with 5% CO_2. Afterward, we observed the quantity and state of the cells under an optical microscope (DM1000, Leica, Wetzlar, Germany) and sub-cultured the cells when seeing that the density of cells attached to the well wall exceeded 80%.

2.2 Transfection of Cells

RiboBio Co., Ltd. (Guangzhou, Guangdong, China) synthesized and provided the short hairpin RNA UBR7 (sh-UBR7, sense 5′-GGAAGTCCTTTCAGTTGATAT-3′, antisense 5′-ATATCAACTGAAAGGACTTCC-3′), and its negative control (sh-NC), UBR7 overexpression plasmid (UBR7, NM_175748) and its negative control (vector), sh-PKM2 (sense: 5′-CCGGGCCCGAGGCTTCTTCAAGAAGTTCAAGAGACTTCTTGAAGAAGC CTCGGGCTTTTTTG-3′, antisense: 5′-AATTCAAAAAAGCCCGAGGCTTCTTCAAGAAGTCTCTTGAACT TCTTGAAGAAGCCTCGGGC-3′) and its negative control (sh-NC), 6-phosphofructo-2-kinase/fructose-2,6-biphosphatase 3 (PFKFB3) overexpression plasmid (PFKFB3, NM_004566) and its negative control (vector). Subsequently, following the instructions provided with Lipofectamine 3000 (L3000001, Invitrogen, Austin, TX, USA), we transfected these vectors into HepG2 and Huh-7 cells and then cultivated the cells in an incubator for 48 h.

2.3 Reverse Transcription Quantitative Polymerase Chain Reaction (RT-qPCR) Testing

First, HHL-5 cells and HCC cells Huh-7, Li-7, HCC-LM3, and HepG2 were dosed with the TRIzol reagent kit (DP424, TIANGEN, Beijing, China) to extract the total RNA. RBA concentration and purity were determined using a NanoDrop spectrophotometer (Thermo Fisher Scientific, Waltham, MA, USA). For reverse transcription, 1 μg of total RNA from each sample was used to synthesize cDNA in a 20 μL reaction system using the Prime Script RT reagent kit (RR047A, Takara, Tokyo, Japan), according to the manufacturer's instructions. Followed by, qRT-PCR testing was conducted on a PRISM 7300 RT-PCR system (ABI, Carlsbad, CA, USA) using the TB Green FAST qPCR Kit (CN830S, Takara). The 20 μL qPCR mixture contained 2 μL of diluted cDNA (approximately 50 ng), 10 μL of TB Green Premix, 0.8 μL of each primer (10 μM), and 6.4 μL of nuclease-free water. The amplification protocol was as follows: initial denaturation at 95°C for 30 s, followed by 40 cycles of denaturation at 95°C for 5 s and annealing/extension at 60°C for 30 s. Melting curve analysis was performed after each run to verify the amplification specificity. Finally, the $2^{-\Delta\Delta Ct}$ method was used to work out the mRNA levels of UBR7 and PKM2 in the cells, treating β-actin as the internal control. The primer sequences were designed as follows:

UBR7: F: 5′-GGCCTGCATGAAACGTTGTT-3′; R: 5′-GGCCAAATGTGAACCACACC-3′.
PKM2: F: 5′-CCTGATAGCTCGTGAGGCTG-3′; R: 5′-GTGGAGTGACTTGAGGCTCG-3′.
β-actin: F: 5′-ATCACTATTGGCAACGAGCG-3′; R: 5′-ACTCATCGTACTCCTGCTTG-3′.

2.4 Cell Counting Kit-8 (CCK-8) Assay

HCC cells (Huh-7 and HepG2) were inoculated into a 96-well plate (2.0×10^4 cells/well). After attaching to the well wall, complete medium (100 μL) that contained 10% of CCK-8 reagent (C0038, Beyotime, Shanghai, China) was placed in the well and subsequently incubated for 2 h in a 37°C incubator. OD_{450} values were assessed through a Varioskan LUX microplate reader (VL0000D0, Thermo Fisher Scientific) to calculate cell viability. Cell viability (%) = [(OD value of treatment group − OD value of blank group)/(OD value of control group − OD value of blank group)] × 100%.

2.5 Clone Formation Experiment

Culture dishes containing 10 mL of 37°C culture medium were prepared. Each dish was seeded with Huh-7 and HepG2 cells transfected with sh-NC/sh-UBR7 or vector/UBR7 (100 cells) and rotated gently to disperse the cells evenly. The dishes were placed in a cell incubator (setting: 37°C; 5% CO_2) for two to three weeks of cultivation. The cultivation was ended when visible clones appeared in the dishes. 4% of paraformaldehyde (P6148, Sigma, St Louis, MO, USA) was dosed to the dishes for 20-min fixation of the

colonies. After two washes with PBS solution (0.01 M, pH 7.2), the cells were colored using an appropriate amount of Giemsa stain (C0133, Beyotime) for 30 min at 25°C. Finally, cells were imaged with an optical microscope (DM1000, Leica, Wetzlar, Germany); the cell clones were then counted, where a colony with more than 50 cells was treated as one clone.

2.6 Scratch-Wound Assay

Added 2 mL of Huh-7 and HepG2 cell suspensions (5×10^5 cells/mL) to a 6-well plate and cultured until reached 90% confluence. With a 100 μL sterile pipette tip perpendicular to the bottom of the 6-well plate wells, a straight line scratch was made in the direction of the well diameter. Subsequently, cells were gently rinsed with PBS (0.01 M, pH 7.2) to clear away cell debris and cultured for 24 h. Using a microscope, the scratch healing was observed, and its width was analyzed through Image J software (1.54 h, National Institutes of Health, Bethesda, MD, USA).

2.7 Transwell Testing

Matrigel (HY-K6002, MedChemExpress, Monmouth Junction, NJ, USA) was melted at 25°C and diluted with RPMI-1640 medium. 100 μL of the diluted gel was aspirated and spread on the bottom of the transwell chamber (8 μm, Corning, Tewksbury, MA, USA), Huh-7 and HepG2 cell suspensions (100 μL) were introduced into the upper chamber, while RPMI-1640 medium (600 μL) was introduced into the lower chamber and incubated at 37°C for 24 h to allow cell growth. Cells were initially treated with 4% paraformaldehyde for 30 min, then dyed with 0.1% crystal violet (HY-B0324A, MedChemExpress) for an additional 30 min. Finally, invasive cells were viewed through a microscope.

2.8 Apoptosis Detection

Huh-7 and HepG2 cells were collected via centrifugation at 5000× *g*, 4°C for 5 min with a centrifuge (H1650R, Xiangyi Laboratory Instrument Development Co., Ltd., Hunan, China), and mixed thoroughly with Binding Buffer (500 μL) provided in the Annexin V-FITC/Propidium Iodide (PI) apoptosis detection kit (HY-K1073, MedChemExpress). After that, 5 μL each of Annexin-V-FITC and PI was introduced, vortexed gently, and incubated for 15 min away from light. Flow cytometry (BD FACSCalibur™, BD Biosciences, San Jose, CA, USA) was applied to detect fluorescence intensity, while the apoptosis rate was quantified via FlowJo software (v10.8, BD Biosciences).

2.9 Testing with Assay Kits

In this part, the absorption level of glucose and the generation levels of lactic acid and ATP in cells were tested with colorimetric methods. Standard and sample dilutions were prepared following the guidelines of the respective assay kits, including the glucose uptake colorimetric assay kit (S0201S, Beyotime), the ATP assay kit (S0026, Beyotime), and the lactic acid colorimetric assay kit (D799851-0050, Sangon, Shanghai, China). After being treated with the assay kits, Huh-7 and HepG2 cells were detected using a multimode microplate reader (Spark, Tecan, Männedorf, Switzerland) to uncover the absorbance of the cells for glucose and lactic acid testing and the chemiluminescence intensity of the cells for ATP testing.

2.10 Experiments In Vivo

Thirty specific pathogen-free (SPF) grade male BALB/c nude mice, aged 5 weeks (15–18 g), were supplied from Model Organisms (Shanghai, China). The mice were housed at a constant temperature of 22 ± 2°C, relative humidity of 45%, and a cycle of 12 h of light and 12 h of darkness. They were acclimatized

to this environment for one week before the experiment. All animal experiments were approved by the Animal Ethics Committee of The First Hospital of China Medical University (Approval No.: 21000025113001) and were strictly performed in accordance with the ARRIVE 2.0 guidelines, with all efforts made to minimize animal suffering. These mice were randomly assigned to five groups (n = 6) using the random number table method, and were subcutaneously injected with 200 μL of the corresponding cell suspension (1.5×10^6 cells) into the right axilla, including untreated Huh-7 cells (Control group), sh-NC-transfected Huh-7 cells, sh-UBR7-transfected Huh-7 cells, empty vector-transfected Huh-7 cells, and UBR7-transfected Huh-7 cells. Every 7 days, the width (W) and length (L) of the tumor were measured to calculate the tumor volume (V) based on the formula of $V = 0.5 \times L \times W^2$ [26]. Tumor volume measurement and subsequent tumor weighing were conducted using a single-blinded procedure, where the investigators responsible for outcome assessment were unaware of the mouse group allocation. The mice underwent euthanasia on the 35th day, and their tumors were carefully separated, followed by weighing and photographing.

2.11 Hematoxylin and Eosin (HE) Staining

Mouse tumor tissues underwent exposure to 4% paraformaldehyde for 24 h, then were dehydrated using graded ethanol (100%, 95%, 75%, and 50%). Subsequently, tissues were embedded in paraffin and prepared into 4 μm sections, deparaffined using xylene (X821391, Macklin, Shanghai, China), and hydrated with graded ethanol. Tissues were dyed with hematoxylin stain solution (C0105S, Beyotime) for 8 min, then treated with differentiation solution (C0161s, Beyotime) for 20 s. Following rinsing with PBS (0.01 M, pH 7.2), sections were dyed with eosin for 60 s, and then dehydrated using gradient ethanol, transparentized with xylene, and observed using a microscope.

2.12 Immunohistochemistry

Paraffin sections of tumor tissue were dewaxed and hydrated, placed in citric acid solution (0.01 M, pH 6.0), and microwaved to repair antigens. Tissues were covered with 3% H_2O_2 solution for 30 min, and blocked using 5% bovine serum albumin (BSA, B2064, Sigma) for 30 min. After that, sections were incubated with Ki67 primary antibody (MA5-14520, 1:100, Invitrogen) at 37°C for 90 min, then exposed to goat anti-rabbit IgG (31460, 1:500, Invitrogen) for 25 min. DAB (HY-W014212, MedChemExpress) was utilized for color development for 10 min, and distilled water was used to terminate the color development. After re-staining using hematoxylin, samples were rinsed with distilled water and observed using a fluorescence microscope (M5000, Invitrogen).

2.13 TUNEL Staining

Tissue sections were dewaxed and hydrated, exposed to DNase-free proteinase K (20 μg/mL, HY-108717A, MedChemExpress) for 30 min, and then washed thoroughly with PBS (0.01 M, pH 7.2). Subsequently, TUNEL solution (C1086, Beyotime) was applied to stain the tissues in darkness for 60 min, and then with DAPI staining solution (C1005, Beyotime) for 10 min. Following covering with AntiFade mounting medium (HY-K1047, MedChemExpress), the samples were photographed using a fluorescence microscope.

2.14 Measurement of Glycolysis Level in Tumor Tissues

After washing the tumor tissues with pre-cooled PBS (0.01 M, pH 7.2), 20 mg of tissue samples were weighed, cut with scissors, and homogenized with 200 μL of NAD^+/NADH extract solution (S0175, Beyotime) on ice using electric homogenizer (JY92-IIN, Ningbo Xinzhi Biotechnology Co., Ltd., Zhejiang, China) at

5000 rpm for 30 s per cycle, with 3 cycles total and 10 sof interval between each cycle to prevent overheating of the homogenate. The tissue homogenate was centrifuged at 8000× *g*, 4°C for 10 min, and the supernatant was carefully collected and transferred to a new sterile EP tube for subsequent NAD+/NADH level detection. Subsequently, standard curves were plotted, and NAD^+/NADH levels were calculated according to the kit instructions. In addition, an ATP assay kit and a lactate dehydrogenase (LDH) assay kit (A020-2-2, Nanjing Jiancheng Bioengineering Institute, Nanjing, China) were applied to detect LDH activity and ATP levels in tumor tissues, with reference to previous studies [27].

2.15 Western Blot

HHL-5 cells and HCC cells Huh-7, Li-7, HCC-LM3, and HepG2 cells were lysed using RIPA lysis buffer (P0039, Beyotime) on ice, followed by centrifugation at 8000× *g*, 4°C for 15 min using a centrifuge (H1650R, Xiangyi Laboratory Instrument Development Co., Ltd.) for protein extraction. The protein content was judged by applying the BCA protein assay kits (P0012) supplied by Beyotime. Protein samples were separated by 10% SDS-PAGE gel electrophoresis, and the proteins were transferred onto a PVDF membrane (88518, Invitrogen). After finishing the translocation, the membrane was incubated with 5% of BSA and blocked for one hour at 25°C. Subsequently, primary antibodies UBR7 (ab305239, 1:1000), phosphoglycerate kinase 1 (PGK1, ab199438, 1:1000), glucose transporter 1 (GLUT1, ab115730, 1:10000), PFKFB3 (ab181861, 1:2000), hexokinase 1 (HK1, ab150423, 1:2000), hexokinase 2 (HK2, ab209847, 1:1000), PKM2 (ab154816, 1:2000), LDHA (ab101562, 1:2000), and β-actin (ab8227, 1:5000) were added to the membrane, staying at 4°C for one night. After a thorough washing with TBST, the membrane was subjected to a 30-min incubation at unregulated temperature with goat anti-rabbit IgG (ab6721, 1:2000). These antibodies were purchased from Abcam (Waltham, MA, USA). After washing with TBST again, the image of protein bands on the membrane was developed by applying ECL (P0018S, Beyotime Biotechnology) and visualized using an imager (5200) produced by Tanon (Shanghai, China). Later, the Image J software was applied for quantitative analysis of the gray values of the protein bands.

2.16 Ubiquitination Assay

HCC cells were treated with a proteasome inhibitor (MG-132, 20 μM, HY-13259, MedChemExpress) for 6 h [23], and then lysed with RIPA lysis buffer for 30 min at 4°C. The lysate was collected, centrifuged, and the supernatant was incubated with PKM2 antibody (ab154816, 1:100, Abcam) overnight at 4°C, with IgG (MA5-42729, 1:100, Invitrogen) as a control. Immunomagnetic beads were added, and incubation was continued at 4°C for 2 h. After centrifugation, the immunoprecipitated complexes were harvested, washed twice with buffer, added to SDS-PAGE uploading buffer, and boiled in a water bath for 10 min. The PKM2 protein supernatant samples were obtained by immunoprecipitation, and ubiquitin antibodies (701339, 1:1000, Invitrogen) were added and incubated, followed by a Western blot to detect ubiquitination of PKM2.

2.17 Data Analysis

The number of samples for the cell experiments was 3 (n = 3), and the number of samples for the animal experiments was 6 (n = 6), with each experiment repeated three times. All sample sizes were analyzed by power analysis using G*Power software with the following parameters: effect size Cohen's f = 0.4, significance level $\alpha = 0.05$, and test efficacy $1-\beta = 0.8$, which was calculated to be 6 samples per group for the animal experiment; For the cellular experiment, the number of independent replicates was set at n = 3 by combining the results of previous studies [23] and pre-tests. Data obtained from the above testing were processed using the SPSS 26.0 software (SPSS Inc., Chicago, IL, USA) and denoted as mean ± standard

deviation. Verification of data normality was performed by the Shapiro-Wilk test, and the Levene test evaluated the homogeneity of variance. The difference between the two groups was assessed by *t*-test, and that among more than two groups were assessed by one-way analysis of variance. $^{*}p < 0.05$ signifies statistical significance.

3 Results

3.1 Overexpression of UBR7 Hinders Proliferation, Invasion, Migration and Induces Apoptosis in HCC Cells

To investigate the involvement of UBR7 with HCC, its expression in HCC cell lines (Li-7, HCC-LM3, Huh-7, and HepG2) and normal liver cells HHL-5 was initially analyzed based on the qRT-PCR and western blot outcomes. In consequence, UBR7 expression levels were apparently reduced in HCC cells, especially in Huh-7 and HepG2 cells ($p < 0.001$, Fig. 1A–C). In light of this, we selected HepG2 and Huh-7 cells for subsequent assays. We transfected sh-NC/sh-UBR7, Vector/UBR7 into these two cells and found that transfection of sh-UBR7 successfully decreased UBR7 expression ($p < 0.001$), while transfection of UBR7 successfully increased UBR7 expression (Fig. 1D–I). As indicated by CCK-8 assay results, transfection of sh-UBR7 significantly increased cell viability, while transfection of UBR7 resulted in decreased viability (Fig. 1J,K). By clone formation assay, it was observed that transfection of sh-UBR7 caused a significant increase in the proliferative capacity ($p < 0.001$), while transfection of UBR7 attenuated the proliferative capacity (Fig. 1L–N). The results of the scratch assay (Fig. 1O–Q) and Transwell assay (Fig. 1R–T) showed that transfection of sh-UBR7 significantly increased the cell migration rate and invading cells ($p < 0.001$), while transfection of UBR7 decreased the migration and invasion ability. Flow cytometry assay revealed that transfection of sh-UBR7 caused a significant decline in apoptosis rate of HCC cells ($p < 0.001$), while transfection of UBR7 increased the apoptosis rate (Fig. 1U–W). These experimental results clearly demonstrated that overexpression of UBR7 inhibited the malignant biological behavior of HCC cells, implying that it may play an oncogenic role in HCC progression.

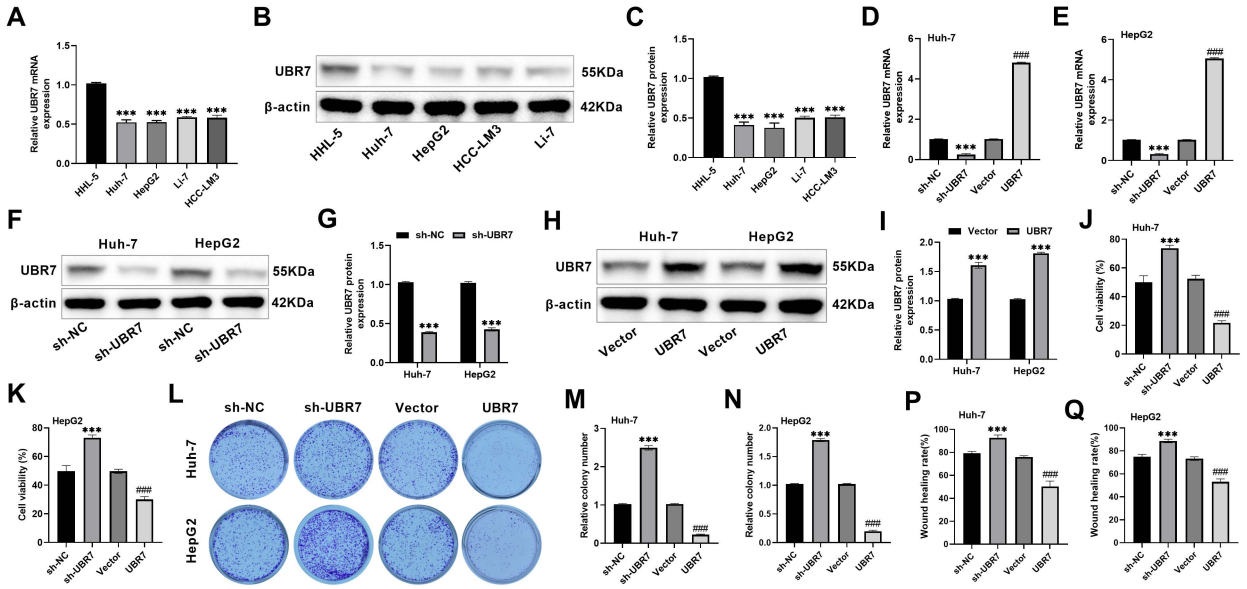

Figure 1: *Cont.*

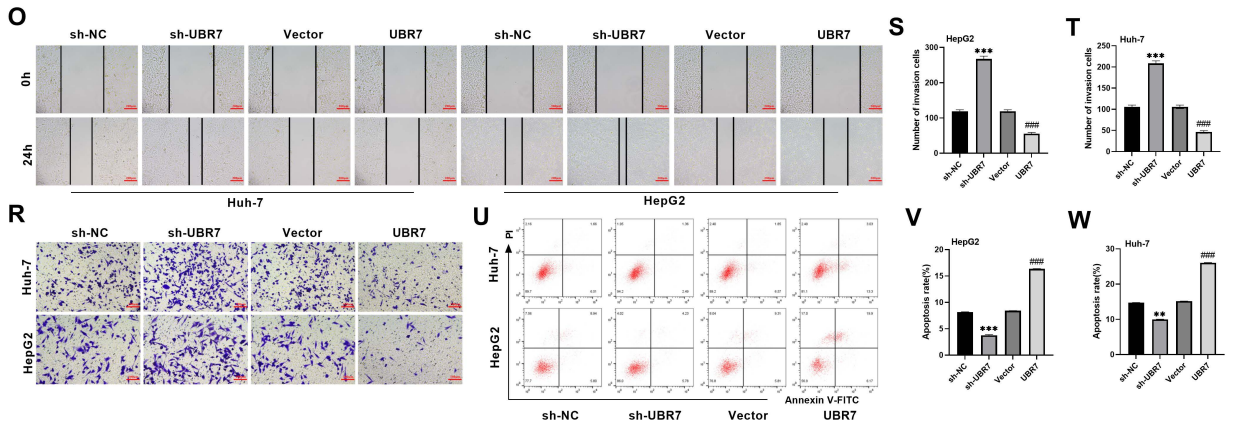

Figure 1: Overexpression of UBR7 hinders proliferation, invasion, migration, and triggers apoptosis in HCC cells. (**A**): UBR7 mRNA expression in HHL-5, Huh-7, HepG2, HCC-LM3, and Li-7 cells was detected using qRT-PCR. (**B**,**C**): UBR7 protein level in the said three cells was revealed through Western blot. (**D**,**E**): qRT-PCR detection of UBR7 mRNA expression after transfection with sh-NC/sh-UBR7 and Vector/UBR7. (**F**–**I**): Western blot detection of UBR7 level in HCC cells after transfection with sh-NC/sh-UBR7, Vector/UBR7. (**J**,**K**): CCK-8 assay for HCC cell activity after overexpression or silencing of UBR7. (**L**–**N**): Multiplication capacity of the said two cells revealed by clone formation experiments. (**O**–**Q**): Scratch assay to detect the migratory ability of HCC cells (10×, 200 μm). (**R**–**T**): Invasion capacity of the two said cells revealed by transwell tests (20×, 100 μm). (**U**–**W**): Flow cytometry detection of apoptosis after silencing or overexpression of UBR7. n = 3. $^{**}p < 0.01$, $^{***}p < 0.001$ vs. sh-NC; $^{\#\#\#}p < 0.001$ vs. Vector.

3.2 Overexpression of UBR7 Inhibits the Glycolysis Level in HCC Cells

Glycolysis is a fundamental characteristic of cancer. Its occurrence drives the absorption of glucose and the generation of ATP and lactic acid. The energy supply to tumor cells in rapid proliferation relies on glycolysis; the ATP generated from glycolysis can quickly supply energy for the synthesis of tumor cells and macromolecules, creating an acidic atmosphere that facilitates tumor advancement [9,28]. Considering PFKFB3's critical role as a glycolysis activator [29], we transfected PFKFB3 into HepG2 and Huh-7 cells and found that the PFKFB3 level was markedly elevated ($p < 0.001$), which could be used for subsequent experiments (Fig. 2A,B). After transfection of sh-UBR7, the absorption of glucose and the generation of lactic acid and ATP in HCC cells were intensified. In contrast, all three indices were significantly reduced after transfection with UBR7 ($p < 0.001$), but PFKFB3 overexpression reduced the inhibitory effect of UBR7 overexpression on glycolysis (Fig. 2C–E). In addition, knockdown of UBR7 notably increased GLUT1, HK1, HK2, PGK1, and LDHA levels, whereas overexpression of UBR7 reversed the trends of these proteins ($p < 0.001$), but overexpression of PFKFB3 reduced the effect of UBR7 overexpression (Fig. 2F–K). This variation denotes that overexpression of UBR7 hinders glycolysis in HCC cells.

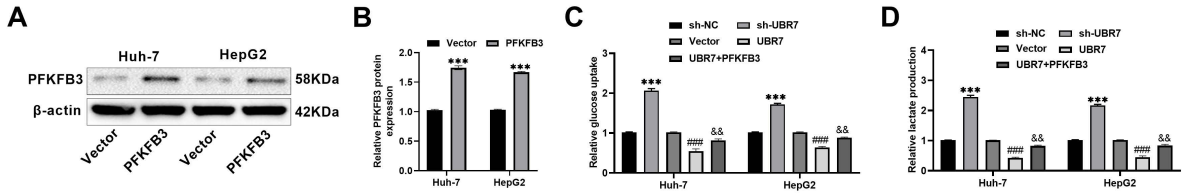

Figure 2: *Cont.*

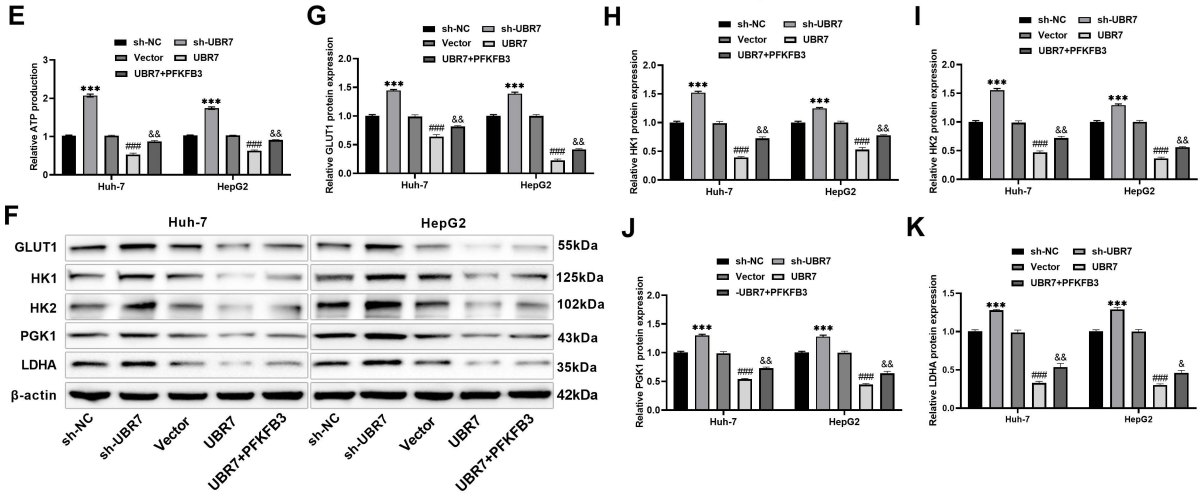

Figure 2: Overexpression of UBR7 inhibits glycolysis level in HCC cells. (**A**,**B**): Western blot detection of PFKFB3 level in Huh-7 and HepG2 cells after transfection with Vector/PFKFB3. (**C**–**E**): The glucose uptake and the production levels of lactic acid and ATP in the said two cells were revealed by using colorimetric assay kits. (**F**–**K**): GLUT1, HK1, HK2, PGK1, and LDHA protein expressions of UBR7 in the said two cells were revealed by western blot. n = 3. $^{***}p < 0.001$ vs. sh-NC; $^{\#\#\#}p < 0.001$ vs. Vector; $^{\&}p < 0.05$, $^{\&\&}p < 0.01$ vs. UBR7.

3.3 Overexpression of UBR7 Inhibits PKM2 Expression in HCC Cells

Given that PKM2 is a principal controller in the aerobic glycolysis process within tumor cells [30], we analyzed the involvement of UBR7 in PKM2 expression. Following the knockdown of UBR7, the PKM2 expression in HCC cells was amplified ($p < 0.001$, Fig. 3A–C); conversely, the PKM2 expression in such cells became depressed following the intensification of UBR7 expression ($p < 0.001$, Fig. 3D–F). Compared with the sh-NC group, PKM2 protein levels were significantly increased in sh-UBR7 cells, suggesting that knockdown of UBR7 increased the stability of PKM2 protein. sh-UBR7 cells showed a further increase in PKM2 protein levels after MG132 treatment, suggesting that UBR7 promotes the degradation of PKM2 protein through the ubiquitin-proteasome pathway ($p < 0.01$, Fig. 3G,H). In addition, knockdown of UBR7 resulted in a decrease in E3 ubiquitin ligase activity and an attenuated ubiquitination modification of PKM2 compared with the sh-NC group (Fig. 3I). This outcome indicates that UBR7 can retard the expression of PKM2 and this retarding effect may be the reason why UBR7 inhibits glycolysis in HCC cells.

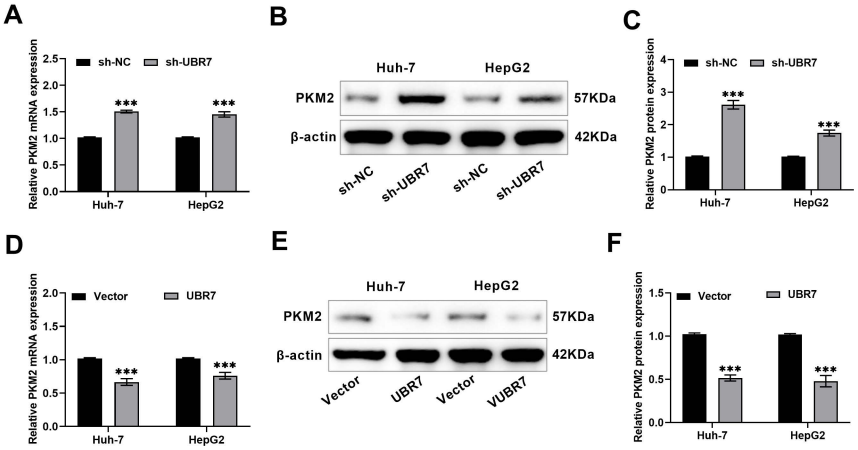

Figure 3: *Cont.*

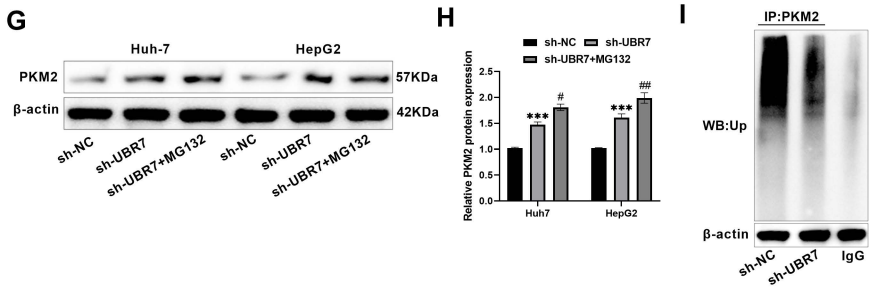

Figure 3: PKM2 expression in HCC cells affected by UBR7. (**A**): mRNA expressions of PKM2 in HepG2 and Huh-7 cells following UBR7 knockdown were revealed by qRT-PCR. (**B**,**C**): PKM2 level in the said two cells following UBR7 knockdown revealed by western blot. (**D**): PKM2 mRNA expressions in the HepG2 and Huh-7 cells following UBR7 overexpression were revealed using qRT-PCR. (**E**,**F**): PKM2 protein level in the said two cells following UBR7 overexpression, as revealed by western blot. (**G**,**H**): After MG132 treatment, PKM2 protein levels were detected by Western blot in HCC cells transfected with sh-UBR7. (**I**): Western blot detection of ubiquitination level of PKM2 protein in HepG2 and Huh-7 cells after transfection with sh-NC or sh-UBR7. n = 3. $^{***}p < 0.001$ vs. sh-NC; $^{\#}p < 0.05$, $^{\#\#}p < 0.01$ vs. sh-UBR7.

3.4 Knockdown of PKM2 Attenuates the Promotional Impact of Knockdown of UBR7 on Malignant Biological Behavior and Glycolysis in HCC Cells

To verify the potential regulatory mechanism between UBR7 and PKM2, rescue experiments were conducted. Knockdown of UBR7 resulted in enhanced clone formation ability (Fig. 4A,B), invasion and migration (Fig. 4C–F), and reduced apoptosis (Fig. 4G,H) in HCC cells; however, this effect of UBR7 knockdown was counteracted in part by the depression of PKM2 ($p < 0.001$). In addition, in HCC cells, knockdown of UBR7 significantly raised glucose uptake, lactate production, and ATP production ($p < 0.001$); whereas knockdown of PKM2 reduced the effect of knockdown of UBR7 (Fig. 4I–K). This suggests that knockdown of PKM2 attenuates the promotional effect of knockdown of UBR7 on the malignant biological characteristics and glycolysis processes of HCC cells.

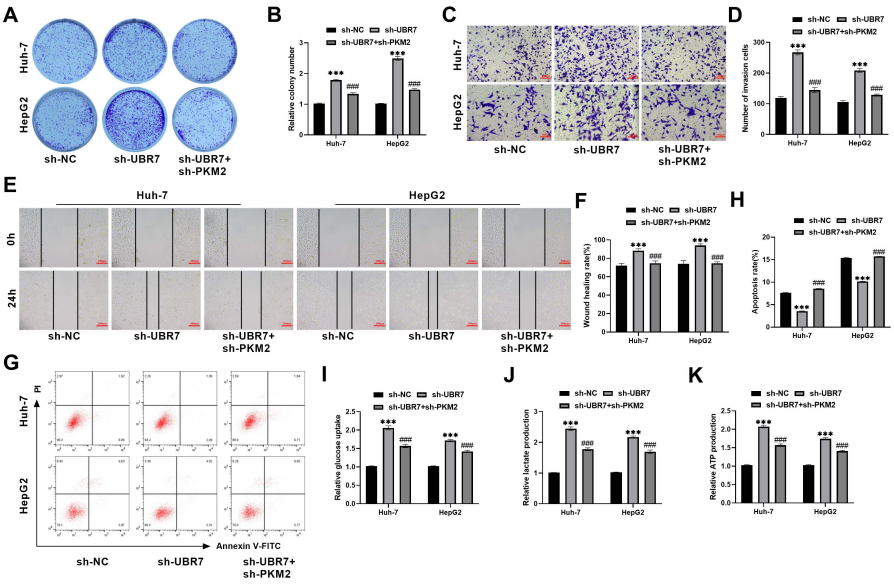

Figure 4: Knockdown of PKM2 attenuates the promotional effect of knockdown of UBR7 on malignant biological behavior and glycolysis in HCC cells. (**A**,**B**): Multiplication capacity of HCC cells revealed by clone

formation experiments. (**C**,**D**): Invasion capacity of the said two cells revealed by the transwell (20×, 100 μm). (**E**,**F**): Scratch assay to assess the migratory ability of HCC cells (10×, 200 μm). (**G**,**H**): Flow cytometry detection of apoptosis in HCC cells. (**I**): The absorption level of glucose in the said two cells was revealed by using glucose uptake colorimetric assay kits. (**J**): The generation levels of lactic acid in the said two cells were revealed by using lactic acid colorimetric assay kits. (**K**): The generation levels of ATP in the said two cells were revealed by using ATP assay kits. n = 3. $^{***}p < 0.001$ vs. sh-NC; $^{\#\#\#}p < 0.001$ vs. sh-UBR7.

3.5 Overexpression of PKM2 Reduces the Inhibitory Impact of Overexpression of UBR7 on the Malignant Progression and Glycolysis of HCC Cells

Next, we explored whether overexpression of PKM2 reduced the effect of overexpression of UBR7. Overexpression of UBR7 resulted in reduced clone formation ability (Fig. 5A,B), invasion and migration (Fig. 5C–F), and reduced apoptosis (Fig. 5G,H) in HCC cells; however, this effect of UBR7 overexpression was counteracted in part by the overexpression of PKM2 ($p < 0.05$). In addition, glucose uptake, lactate production, and ATP production were significantly reduced in HCC cells after overexpression of UBR7 ($p < 0.01$); whereas overexpression of PKM2 reduced the suppressive impact of overexpression of UBR7 on glycolysis (Fig. 5I–K). These consequences suggest that PKM2 can mitigate the effects of UBR7 on cellular biological processes and aerobic glycolysis; PKM2 is likely a target molecule of UBR7. By impeding PKM2, UBR7 exerts its effect to dampen the expansion of HCC.

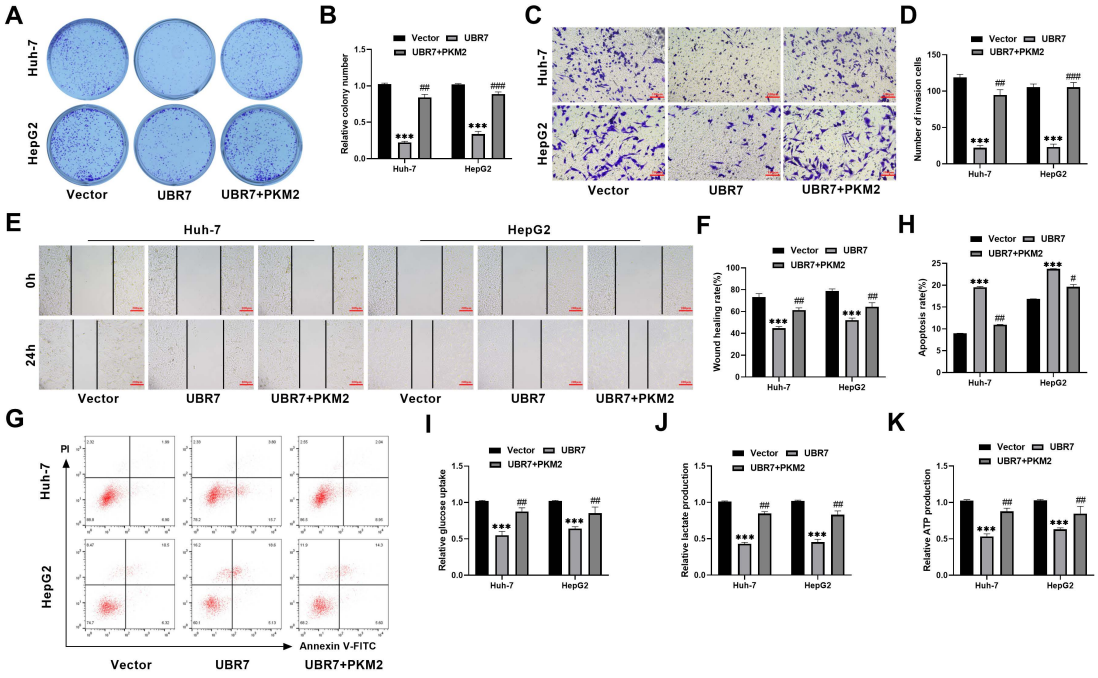

Figure 5: Overexpression of PKM2 attenuates the inhibitory effect of overexpression of UBR7 on the malignant biological behavior and glycolysis of HCC cells. (**A**,**B**): Multiplication capacity of HepG2 and Huh-7 cells revealed by clone formation experiments. (**C**,**D**): Invasion capacity of the said two cells revealed by the transwell assay (20×, 100 μm). (**E**,**F**): Scratch assay to detect cell migratory ability (10×, 200 μm). (**G**,**H**): Flow cytometry detection of apoptosis in HCC cells. (**I**): The absorption level of glucose in the said two cells was revealed by using glucose uptake colorimetric assay kits. (**J**): The generation levels of lactic acid in the said two cells were revealed by using lactic acid colorimetric assay kits. (**K**): The generation levels of ATP in the said two cells were revealed by using ATP assay kits. n = 3. $^{***}p < 0.001$ vs. Vector; $^{\#}p < 0.05$, $^{\#\#}p < 0.01$, $^{\#\#\#}p < 0.001$ vs. UBR7.

3.6 Overexpression of UBR7 Inhibits PKM2 Expression and Suppresses Tumor Growth In Vivo

To make clear the practical impact of UBR7 in HCC conditions, HCC xenograft models were created in nude mice. UBR7 was down-regulated, and PKM2 was up-regulated in tumor tissues of the sh-UBR7 group, whereas UBR7 was up-regulated and PKM2 was down-regulated in tumor tissues of the UBR7 group ($p < 0.01$, Fig. 6A–C). Knockdown of UBR7 significantly increased tumor volume and weight, while UBR7 overexpression inhibited tumor growth ($p < 0.001$, Fig. 6D–F). As viewed through HE staining, knockdown of UBR7 still maintained a high cell density in tumor tissues; whereas overexpression of UBR7 resulted in a looser arrangement of cells (Fig. 6G). Immunohistochemistry findings indicated that UBR7 knockdown increased Ki-67 levels; whereas UBR7 overexpression caused a decline in Ki-67 levels, suggesting that UBR7 overexpression hindered the proliferation of tumor cells ($p < 0.001$, Fig. 6H,I). TUNEL staining showed that UBR7 knockdown decreased the TUNEL-positive rate in tumor tissues; whereas UBR7 overexpression increased the positive rate, suggesting that overexpression of UBR7 induced apoptosis in tumor cells ($p < 0.001$, Fig. 6J,K). These results suggest that overexpression of UBR7 inhibits PKM2 expression and suppresses tumor growth in nude mice *in vivo*.

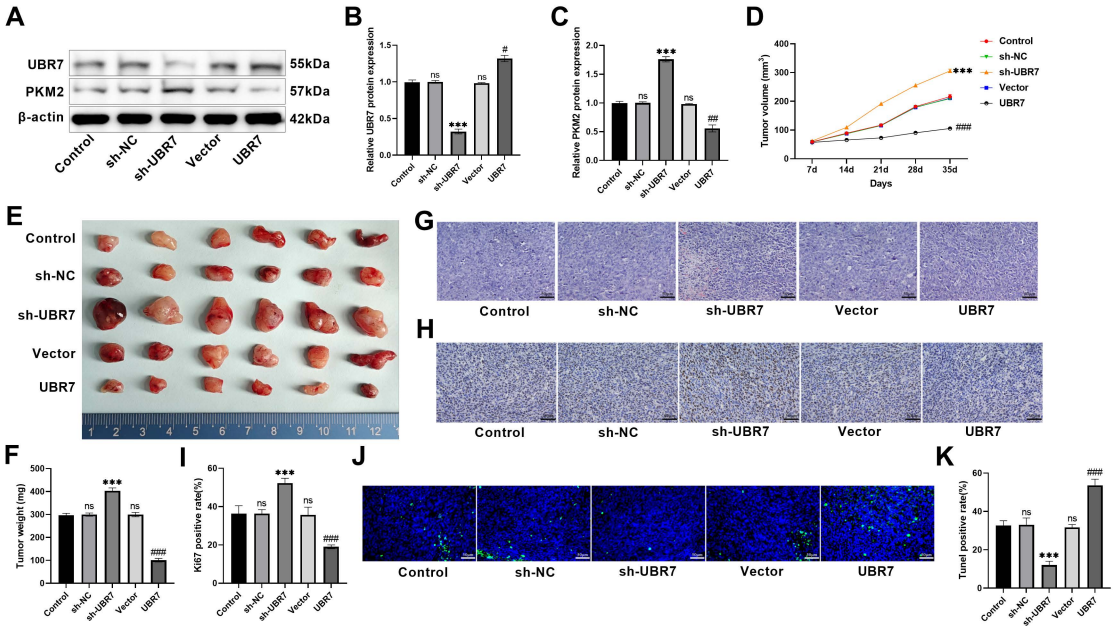

Figure 6: Overexpression of UBR7 inhibits PKM2 expression and thus tumor growth *in vivo*. (**A**–**C**): Protein expressions of UBR7 and PKM2 in the tumor tissues were revealed by Western blot. (**D**): Every week, the dimensions of tumors were assessed. (**E**,**F**): The tumors were weighed on the 35th day. (**G**): Tumor histopathological changes observed by HE staining (40×, 50 μm). (**H**,**I**): Assessing Ki-67 levels in tumor tissues using immunohistochemistry (40×, 50 μm). (**J**,**K**): TUNEL staining confirmed that overexpression of UBR7 the TUNEL-positive cell rate (40×, 50 μm). n = 6. ns $p \geq 0.05$ vs. Control; $^{***}p < 0.001$ vs. sh-NC; $^{\#}p < 0.05$, $^{\#\#}p < 0.01$, $^{\#\#\#}p < 0.001$ vs. Vector.

3.7 UBR7 Reduces Tumor Cell Glycolysis In Vivo by Inhibiting PKM2 Expression

To make clear the practical effect of UBR7 in HCC conditions, HCC xenograft models were created in nude mice. Knockdown of UBR7 significantly increased ATP concentration, LDH activity, and the relative NAD^+/NADH ratio in tumor tissues ($p < 0.05$). Conversely, UBR7 overexpression led to a marked decrease in these three indicators (Fig. 7A–C). Additionally, UBR7 knockdown upregulated GLUT1, HK1, HK2, PGK1,

and LDHA levels in tumor tissues, whereas UBR7 overexpression downregulated these glycolysis-related proteins ($p < 0.05$, Fig. 7D–I). Collectively, these findings demonstrate that UBR7 reduces the glycolytic activity of tumor cells *in vivo* by hindering PKM2 expression.

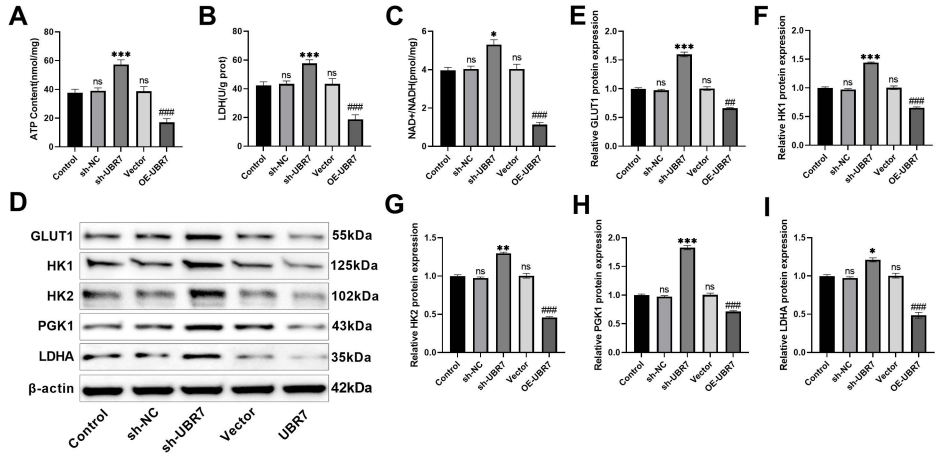

Figure 7: UBR7 reduces tumor cell glycolysis *in vivo* by inhibiting PKM2 expression. (**A**–**C**): Detection of ATP concentration, LDH activity, and relative NAD^+/NADH ratio in tumor tissues using ATP assay kit, LDH assay kit, and NAD+/NADH assay kit. (**D**–**I**): GLUT1, HK1, HK2, PGK1, and LDHA protein levels in the tumor tissues were assessed using Western blot. n = 6. ns $p \geq 0.05$ vs. Control; $^{*}p < 0.05$, $^{**}p < 0.01$, $^{***}p < 0.001$ vs. sh-NC; $^{\#\#}p < 0.01$, $^{\#\#\#}p < 0.001$ vs. Vector.

4 Discussion

Our research confirmed the impending impacts of UBR7 on the multiplication and migration of HCC cells (Huh-7 and HepG2), alongside suppressing tumor growth *in vivo*. PKM2, being a key regulator in the aerobic glycolysis of cells, can partially reverse UBR7's suppression of the exacerbation of HCC cells and is inversely regulated by UBR7. Therefore, it was hypothesized that UBR7's suppression of HCC might have a relation with the path of aerobic glycolysis. According to the generation levels of lactic acid and ATP and the absorption level of glucose detected in cells with different levels of UBR7, UBR7 was proven to be inhibitory for cellular aerobic glycolysis. The underlying reason may be that UBR7-mediated downregulation of PKM2 impairs the final step of glycolysis, reducing energy production and metabolic intermediates required for HCC cell malignant progression, thereby exerting an anti-tumor effect. In terms of mechanism, UBR7 suppressed the PKM2-mediated way of cellular aerobic glycolysis, impairing the development of HCC.

Ubiquitination is a highly conserved pathway for post-translational modification of proteins in eukaryotic cells [31]. During ubiquitination, the E3 ubiquitin ligase selectively transfers E2 to the substrate, determining the specific recognition of target proteins [32–34]. The UBR family, representing a unique category of E3 ubiquitin ligases, has a zinc finger-like UBR box domain comprising 70 residues. It can recognize N-degrons and induce protein degradation [35,36]. Up to now, UBR1-7 have been identified in mammals. Among them, UBR7 is distinct from other UBR proteins; the C-terminus of UBR7 contains a plant homeodomain, which aids in the reading of histone codes [35,37]. This structural feature implies that UBR7 may regulate gene expression through both ubiquitin-mediated protein degradation and histone modification, providing a potential molecular basis for its negative regulation of PKM2. Whereas the effects of UBR7 in tumor development are poorly understood due to insufficient research on UBR7. Through this work, we know that UBR7 is effective in alleviating the multiplication, migration, and aerobic glycolysis of

HCC cells and hindering HCC tumor growth in mice; besides, UBR7 can inversely regulate the PKM2 gene in HCC cells, which may be a way by which UBR7 modulates the exacerbation and aerobic glycolysis of such cells. Notably, our findings are consistent with a previous study reporting that UBR7 alleviates HCC progression by impairing glycolysis [31], further validating the reliability of our results and highlighting the conserved role of UBR7 in HCC metabolic regulation.

The liver is the main organ for glucose and fat metabolism. In case of liver damage, the metabolic balance is broken, resulting in carcinogenesis. In this process, tumor cells tend to rely on glycolysis, a pathway 15 times more efficient than aerobic respiration in glucose metabolism, to meet the energy and anabolism demands of their excessive proliferation [38,39]. Featured by the magnified absorption of glucose and the generation of ATP and lactic acid [40–42], aerobic glycolysis can drive the vascularization, immune evasion, metastasis, and proliferation in HCC cells [43]. According to the testing results acquired in this survey, Huh-7 and HepG2 cells experienced greatly depressed absorption of glucose and generation of ATP and lactic acid when UBR7 was excessively expressed; whereas, the opposite outcomes were observed when UBR7 was leveled down; moreover, regulating the PKM2 gene level up helped to the glucose absorption, ATP and lactic acid generation in HCC cells and retarded the effect of UBR7. These results collectively indicate that UBR7 inhibits aerobic glycolysis in HCC cells by downregulating PKM2, which disrupts the metabolic reprogramming of HCC cells, cuts off the energy supply for malignant progression, and ultimately exerts anti-HCC effects.

Several potential limitations need to be acknowledged. *In vitro* experiments only used two HCC cell lines (Huh-7 and HepG2), which failed to cover HCC cells of different differentiation degrees and pathological subtypes, and thus may not fully reflect the regulatory role of UBR7 in various types of HCC. In addition, the *in vivo* experiments in this study did not construct a hepatocellular carcinoma metastasis model and failed to verify the effect of UBR7 on the metastatic process of HCC *in vivo*. Based on the above limitations, we will further expand the selection of cell lines and adopt various liver cancer models to improve the experimental validation; at the same time, we will construct a liver cancer metastasis model by tail vein injection to investigate whether UBR7 can regulate the migration and invasion ability of tumor cells to inhibit the metastatic process of liver cancer *in vivo*. Besides, in the future, the correlation between the expression of UBR7 and PKM2 and its predictive value for patients' prognosis will be verified by combining with clinical samples testing, and the cross-talk between the UBR7-PKM2 axis and the tumor glycolysis-related pathways (e.g., PI3K/AKT pathway) will be further explored with the aim of deepening the understanding of the regulatory mechanism of glycolysis in hepatocellular carcinoma, and completing the conclusions and the mechanistic network of the present study.

5 Conclusion

In summary, UBR7 may suppress aerobic glycolysis by targeted regulation of PKM2, thus retarding the progression of HCC, whereas this effect depends on UBR7's suppression of PKM2. This paper puts forward a viable way of inhibiting HCC based on the resistance to glycolysis. However, PKM2 modulates a variety of complex cellular events, and UBR7 can target glycolysis through numerous pathways. It is still needed to identify the action target of UBR7 to better understand the mechanism of UBR7 in modulating HCC and propel the application of UBR7 in treating malignant tumors.

Acknowledgement: None.

Funding Statement: The authors received no specific funding for this study.

Author Contributions: [Bo Liu, Xue Li]: Conceived and designed the research, and analyzed data. Drafted and revised the manuscript critically for important intellectual content. [Bo Liu, Xue Li]: Contributed to the acquisition, analysis, and interpretation of data. Provided substantial intellectual input during the drafting and revision of the manuscript. [Xue Li]: Participated in the conception and design of the study. Played a key role in data interpretation and manuscript preparation. All authors reviewed and approved the final version of the manuscript.

Availability of Data and Materials: The data supporting the findings of this study can be obtained from the corresponding author upon request.

Ethics Approval: This study was reviewed and approved by the Animal Ethics Committee of The First Hospital of China Medical University (Approval No.: 21000025113001).

Conflicts of Interest: The authors declare no conflicts of interest.

References

1. Sung H, Ferlay J, Siegel RL, Laversanne M, Soerjomataram I, Jemal A, et al. Global cancer statistics 2020: GLOBOCAN estimates of incidence and mortality worldwide for 36 cancers in 185 countries. CA Cancer J Clin. 2021;71(3):209–49. [CrossRef].
2. Kim E, Viatour P. Hepatocellular carcinoma: Old friends and new tricks. Exp Mol Med. 2020;52(12):1898–907. [CrossRef].
3. Yuan H, Xia C, Zhang J, Wang S, Sun J, Yan S, et al. Ciclopirox, a broad-spectrum antifungal drug, moonlights as a pyroptosis agonist to drive hepatocellular carcinoma cell death. Eur J Pharmacol. 2025;1008:178358. [CrossRef].
4. Yeo YH, Abdelmalek M, Khan S, Moylan CA, Rodriquez L, Villanueva A, et al. Current and emerging strategies for the prevention of hepatocellular carcinoma. Nat Rev Gastroenterol Hepatol. 2025;22(3):173–90. [CrossRef].
5. Mu R, Chang M, Feng C, Cui Y, Li T, Liu C, et al. Analysis of the expression of PRDX6 in patients with hepatocellular carcinoma and its effect on the phenotype of hepatocellular carcinoma cells. Curr Genomics. 2024;25(1):2–11. [CrossRef].
6. Wang L, Zhu Z, Liang Q, Tao Y, Jin G, Zhong Y, et al. A novel small molecule glycolysis inhibitor WZ35 exerts anti-cancer effect via metabolic reprogramming. J Transl Med. 2022;20(1):530. [CrossRef].
7. Jin HR, Wang J, Wang ZJ, Xi MJ, Xia BH, Deng K, et al. Lipid metabolic reprogramming in tumor microenvironment: From mechanisms to therapeutics. J Hematol Oncol. 2023;16(1):103. [CrossRef].
8. Barba I, Carrillo-Bosch L, Seoane J. Targeting the Warburg effect in cancer: Where do we stand? Int J Mol Sci. 2024;25(6):3142. [CrossRef].
9. Paul S, Ghosh S, Kumar S. Tumor glycolysis, an essential sweet tooth of tumor cells. Semin Cancer Biol. 2022;86(Pt 3):1216–30. [CrossRef].
10. Upadhyay M, Samal J, Kandpal M, Singh OV, Vivekanandan P. The Warburg effect: Insights from the past decade. Pharmacol Ther. 2013;137(3):318–30. [CrossRef].
11. Zhao M, Wei F, Sun G, Wen Y, Xiang J, Su F, et al. Natural compounds targeting glycolysis as promising therapeutics for gastric cancer: A review. Front Pharmacol. 2022;13:1004383. [CrossRef].
12. Wong N, Ojo D, Yan J, Tang D. PKM2 contributes to cancer metabolism. Cancer Lett. 2015;356(2 Pt A):184–91. [CrossRef].
13. Zhu S, Guo Y, Zhang X, Liu H, Yin M, Chen X, et al. Pyruvate kinase M2 (PKM2) in cancer and cancer therapeutics. Cancer Lett. 2021;503:240–8. [CrossRef].
14. Gui DY, Lewis CA, Vander Heiden MG. Allosteric regulation of PKM2 allows cellular adaptation to different physiological states. Sci Signal. 2013;6(263):pe7. [CrossRef].
15. Prasetyanti PR, Medema JP. Intra-tumor heterogeneity from a cancer stem cell perspective. Mol Cancer. 2017;16(1):41. [CrossRef].
16. Wang S, Zhang T, Zhou Y, Jiao Z, Lu K, Liu X, et al. GP73-mediated secretion of PKM2 and GP73 promotes angiogenesis and M2-like macrophage polarization in hepatocellular carcinoma. Cell Death Dis. 2025;16:69. [CrossRef].

17. Liu W, Wu J, Zhang X, Zhang Y, Zeng X, Peng X. PKM2 orchestrates tumor progression via metabolic reprogramming and MDSCs-mediated immune suppression in the tumor microenvironment. Front Immunol. 2025;16:1588019. [CrossRef].
18. Zhang W, Zhang X, Huang S, Chen J, Ding P, Wang Q, et al. FOXM1D potentiates PKM2-mediated tumor glycolysis and angiogenesis. Mol Oncol. 2021;15(5):1466–85. [CrossRef].
19. Liu F, Chen J, Li K, Li H, Zhu Y, Zhai Y, et al. Ubiquitination and deubiquitination in cancer: From mechanisms to novel therapeutic approaches. Mol Cancer. 2024;23(1):148. [CrossRef].
20. Xie Y, Wang M, Xia M, Guo Y, Zu X, Zhong J. Ubiquitination regulation of aerobic glycolysis in cancer. Life Sci. 2022;292:120322. [CrossRef].
21. Hinterndorfer M, Spiteri VA, Ciulli A, Winter GE. Targeted protein degradation for cancer therapy. Nat Rev Cancer. 2025;25(7):493–516. [CrossRef].
22. Xiao Y, Yu TJ, Xu Y, Ding R, Wang YP, Jiang YZ, et al. Emerging therapies in cancer metabolism. Cell Metab. 2023;35(8):1283–303. [CrossRef].
23. Liu S, Liu H, Gong C, Li G, Li Q, Pan Z, et al. miR-10b-5p regulates neuronal autophagy and apoptosis induced by spinal cord injury through UBR7. Neuroscience. 2024;543:13–27. [CrossRef].
24. Singh V, Mondal A, Adhikary S, Mondal P, Shirgaonkar N, DasGupta R, et al. UBR7 E3 ligase suppresses interferon-β mediated immune signaling by targeting Sp110 in hepatitis B virus-induced hepatocellular carcinoma. ACS Infect Dis. 2024;10(11):3775–96. [CrossRef].
25. Feng M, Jiao Q, Ren Y, Liu X, Gao Z, Li Z, et al. The interaction between UBR7 and PRMT5 drives PDAC resistance to gemcitabine by regulating glycolysis and immune microenvironment. Cell Death Dis. 2024;15(10):758. [CrossRef].
26. Shao YY, Chen PS, Lin LI, Lee BS, Ling A, Cheng AL, et al. Low miR-10b-3p associated with sorafenib resistance in hepatocellular carcinoma. Br J Cancer. 2022;126(12):1806–14. [CrossRef].
27. Wang T, Zhang M, Khan M, Li J, Wu X, Ma T, et al. Cryptotanshinone suppresses ovarian cancer via simultaneous inhibition of glycolysis and oxidative phosphorylation. Biomed Pharmacother. 2024;170:115956. [CrossRef].
28. Chelakkot C, Chelakkot VS, Shin Y, Song K. Modulating glycolysis to improve cancer therapy. Int J Mol Sci. 2023;24(3):2606. [CrossRef].
29. Liu Q, Li J, Li X, Zhang L, Yao S, Wang Y, et al. Advances in the understanding of the role and mechanism of action of PFKFB3-mediated glycolysis in liver fibrosis (Review). Int J Mol Med. 2024;54(6):105. [CrossRef].
30. Zhang Z, Deng X, Liu Y, Liu Y, Sun L, Chen F. Correction to: PKM2, function and expression and regulation. Cell Biosci. 2019;9(1):59. [CrossRef].
31. Zhao L, Kang M, Liu X, Wang Z, Wang Y, Chen H, et al. UBR7 inhibits HCC tumorigenesis by targeting Keap1/Nrf2/Bach1/HK2 and glycolysis. J Exp Clin Cancer Res. 2022;41(1):330. [CrossRef].
32. Garcia-Barcena C, Osinalde N, Ramirez J, Mayor U. How to inactivate human ubiquitin E3 ligases by mutation. Front Cell Dev Biol. 2020;8:39. [CrossRef].
33. Jia L, Yan F, Cao W, Chen Z, Zheng H, Li H, et al. Dysregulation of CUL4A and CUL4B ubiquitin ligases in lung cancer. J Biol Chem. 2017;292(7):2966–78. [CrossRef].
34. Wang D, Ma L, Wang B, Liu J, Wei W. E3 ubiquitin ligases in cancer and implications for therapies. Cancer Metastasis Rev. 2017;36(4):683–702. [CrossRef].
35. Adhikary S, Chakravarti D, Terranova C, Sengupta I, Maitituoheti M, Dasgupta A, et al. Atypical plant homeodomain of UBR7 functions as an $H_2BK_{120}Ub$ ligase and breast tumor suppressor. Nat Commun. 2019;10(1):1398. [CrossRef].
36. Choi WS, Jeong BC, Joo YJ, Lee MR, Kim J, Eck MJ, et al. Structural basis for the recognition of N-end rule substrates by the UBR box of ubiquitin ligases. Nat Struct Mol Biol. 2010;17(10):1175–81. [CrossRef].
37. Kim JG, Shin HC, Seo T, Nawale L, Han G, Kim BY, et al. Signaling pathways regulated by UBR box-containing E3 ligases. Int J Mol Sci. 2021;22(15):8323. [CrossRef].
38. Koppenol WH, Bounds PL, Dang CV. Otto Warburg's contributions to current concepts of cancer metabolism. Nat Rev Cancer. 2011;11(5):325–37. [CrossRef].
39. Li X, Ramadori P, Pfister D, Seehawer M, Zender L, Heikenwalder M. The immunological and metabolic landscape in primary and metastatic liver cancer. Nat Rev Cancer. 2021;21(9):541–57. [CrossRef].

40. Brooks GA. Lactate as a fulcrum of metabolism. Redox Biol. 2020;35:101454. [CrossRef].
41. Chang CH, Qiu J, O'Sullivan D, Buck MD, Noguchi T, Curtis JD, et al. Metabolic competition in the tumor microenvironment is a driver of cancer progression. Cell. 2015;162(6):1229–41. [CrossRef].
42. Reinfeld BI, Rathmell WK, Kim TK, Rathmell JC. The therapeutic implications of immunosuppressive tumor aerobic glycolysis. Cell Mol Immunol. 2022;19(1):46–58. [CrossRef].
43. Feng J, Li J, Wu L, Yu Q, Ji J, Wu J, et al. Emerging roles and the regulation of aerobic glycolysis in hepatocellular carcinoma. J Exp Clin Cancer Res. 2020;39(1):126. [CrossRef].